Cross-frequency synchronization of oscillators with time-delayed coupling

Vladimir V. Klinshov,* Dmitry S. Shchapin, and Vladimir I. Nekorkin
Institute of Applied Physics of the Russian Academy of Sciences, 46 Ul'yanov Street, 603950, Nizhny Novgorod, Russia
and University of Nizhny Novgorod, 23 Prospekt Gagarina, 603950, Nizhny Novgorod, Russia
(Received 3 September 2014; published 28 October 2014)

We carry out theoretical and experimental studies of cross-frequency synchronization of two pulse oscillators with time-delayed coupling. In the theoretical part of the paper we utilize the concept of phase resetting curves and analyze the system dynamics in the case of weak coupling. We construct a Poincaré map and obtain the synchronization zones in the parameter space for $m:n$ synchronization. To challenge the theoretical results we designed an electronic circuit implementing the coupled oscillators and studied its dynamics experimentally. We show that the developed theory predicts dynamical properties of the realistic system, including location of the synchronization zones and bifurcations inside them.

DOI: 10.1103/PhysRevE.90.042923 PACS number(s): 05.45.Xt

I. INTRODUCTION

Synchronization of coupled oscillators is a classical nonlinear phenomenon playing an important role in various areas of science including mechanics [1], optics [2], communication and control [3], chemistry [4], and living systems [5]. A striking example of such systems is neural networks. Synchronization of brain areas is believed to be crucial for cognitive functions and to act as an integrative mechanism bringing a widely distributed set of neurons together into a coherent ensemble for a cognitive act [6]. For example, synchronous γ-rate activity of various areas in visual cortex underlies binding of numerous features of an object for its perception [7]. Synchronization is also assumed to be involved in memory and learning [8], motor control [9], and, on the opposite side, in pathologies such as Parkinson's disease or schizophrenia [10]. Recently the role of cross-frequency synchronization between different bands of brain rhythms has been studied as well. This phenomenon is hypothesized to serve as a mechanism for the orienting response and dealing with items in working memory [11].

The presence of coupling delays is an inevitable feature of neural networks as well as many other oscillatory networks. The origin of coupling delays is finite speed of signal propagation in networks and inertness of connections (synapses in the case of neural networks). Numerous theoretical studies demonstrate that the introduction of delayed coupling causes a significant change in network dynamics. Particularly, synchronization properties are sensitive to delays (see the reviews [12]). Delay-induced synchronization and desynchronization were reported, the emergence of multistable synchronous solutions was often observed, and the properties of existing synchronous regimes were shown to be altered after the delay introduction. Theoretical results inspired experimental study of synchronization of oscillators with delayed coupling. Various configurations of interacting lasers were studied with coupling delays arising from the finite speed of light propagation along fibers [13]. Electronic [14] and chemical [15] oscillators have also been considered with delayed coupling realized with the help of digital delay lines.

In this paper we investigate the influence of coupling delays on cross-frequency, or harmonic synchronization. This type of synchronization is observed for oscillatory subsystems with sufficiently different frequencies. Coupling between such subsystems may lead to the emergence of periodical regimes in which the frequencies of the individual oscillators are locked and relate as small integer numbers. For a pair of coupled oscillators this means a relation $f_1 : f_2 = m:n$, for which the regime is called $m:n$ synchronization. Cross-frequency synchronization of oscillators of various nature was a focus of some previous works [16], but the influence of the delays has not been explored sufficiently. In our study we consider two oscillators with time-delayed pulsatile coupling. We systematically study $m:n$ synchronization of the oscillators and obtain analytical criteria for the existence of these regimes in the limit of weak coupling. In order to confirm the obtained theoretical results we developed an electronic circuit implementing the system and explored its dynamics experimentally.

The paper organization is as follows. In Sec. II we introduce our model, provide a mathematical analysis of the synchronization, and obtain the synchronization zones. In Sec. III we describe the experimental setup and the experimental results. In Sec. IV we discuss the results obtained theoretically and experimentally and compare them.

II. THEORETICAL ANALYSIS OF CROSS-FREQUENCY SYNCHRONIZATION

To describe the interaction between the oscillators we use the concept of phase resetting curves (PRCs) [17]. This concept suggests that the interaction between the oscillators consists in exchange of short signals, the so-called pulses. When a pulse from an oscillator is received by another one the phase of the latter one undergoes an instant change. The phase resetting curve defines how much the oscillator is advanced or delayed subject to the magnitude and the timing of the incoming pulse. The concept of pulse-coupled oscillators was used for theoretical study in a number of previous papers [18] in which the authors considered synchronization of delay-coupled networks. The theoretical framework for studying networks with time-delayed pulsatile coupling was developed in [19]. This framework takes advantage of the pulsatile nature of coupling which allows one to focus on discrete events of the system dynamics which occur when the oscillators emit or receive pulses. The same idea is used in the present study.

*vladimir.klinshov@gmail.com

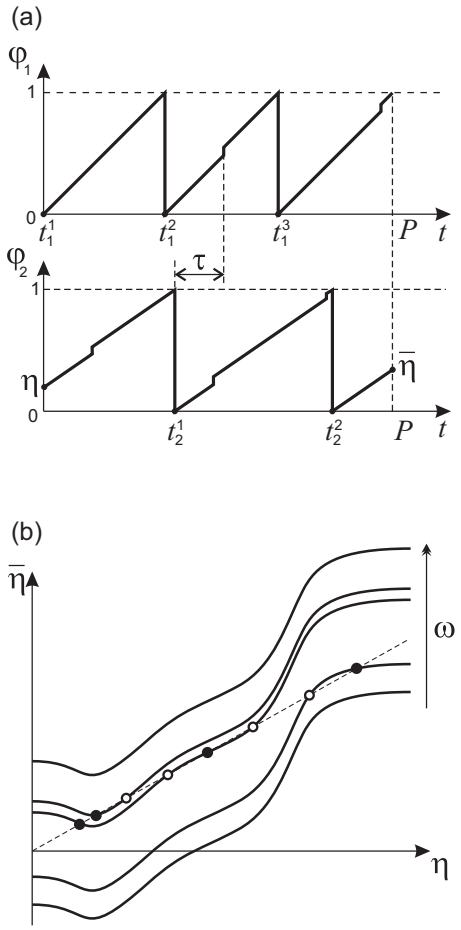

FIG. 1. (a) Dynamics of the system (1). When the phase reaches unity it is reset to zero and the oscillator produces a pulse. Small jumps of the phase correspond to the instants when the oscillator receives delayed pulses from the other oscillator. (b) The return functions of the map (5) for different values of the parameter ω. When ω increases the curve shifts upwards (as depicted by the double arrow) and various fixed points emerge and vanish sequentially. Stable fixed points are plotted by solid circles; unstable ones are plotted by empty circles.

In the current paper we consider a pair of phase oscillators with pulsatile time-delayed coupling. In an autonomous case, each oscillator is described by its phase φ_j which grows uniformly: $d\varphi_j/dt = \omega_j$, where ω_j is the frequency of the oscillator. Each time when the phase reaches the threshold $\varphi_j = 1$ it is reset to zero and the oscillator emits a pulse. The system of two oscillators is governed by the following equations:

$$\frac{d\varphi_j}{dt} = \omega_j + F_j(\varphi_j)\sum_{t_k^p}\delta\left(t - t_k^p - \tau_j\right). \tag{1}$$

Here, $j = 1,2, k = 3 - j, \tau_j$ are the coupling delays, $F_j(\varphi)$ is the phase resetting curve for the jth oscillator, and the sum runs over the instants t_k^p when the kth oscillator produces pulses. The dynamics of the system is illustrated in Fig. 1(a). Each pulse produced by the kth oscillator at the instant t_k^p reaches the jth oscillator at the instant $t_k^p + \tau_j$ and causes a shift of the phase of the latter one $\Delta\varphi_j = F_j(\varphi_j)$. Thus, the phase resetting curve indicates how much the input pulse advances or delays the oscillator. For the sake of certainty we consider the case of symmetric coupling, so that $\tau_1 = \tau_2 = \tau$. We also suppose the phase resetting curve is in the following form: $F_j(\varphi) = \varepsilon\omega_j f(\varphi)$, where ε is the coupling strength. The PRC is set proportional to the oscillator frequency because such type of scaling seems natural for a wide class of oscillators [20] and indeed reveals when realistic oscillators are studied (see Sec. III). We also assume without loss of generality $\omega_1 = 1$, and denote $\omega \equiv \omega_2$.

We define $m:n$ synchronization as a periodical regime when the first oscillator emits m pulses per period and the second one emits n pulses per period, where m and n are incommensurable (further, we suppose $m \geqslant n$). For $m = n = 1$ this means phase locking in the ordinary sense, otherwise it is cross-frequency synchronization. The ratio $m:n$ is also called the rotation number ρ.

Let us study solutions of system (1) corresponding to $m:n$ synchronization. Suppose that $\varphi_1(t = 0) = 0$ and $\varphi_2(t = 0) = \eta$, and the period of the sought-for solution is P. This means that the first (second) oscillator emitted m (n) pulses for $t \in [0; P)$ [such a regime is illustrated in Fig. 1(a) for $m = 3$, $n = 2$]. Denote $t_1^1, t_1^2, \ldots, t_1^m$ the moments when the first oscillator produces pulses, and $t_2^1, t_2^2, \ldots, t_2^n$ the moments when the second one does. Then the moments when the oscillators receive input pulses equal $(t_2^p + \tau) \mod P$, $p = 1,2,\ldots,n$ for the first oscillator, and $(t_1^p + \tau) \mod P$, $p = 1,2,\ldots,m$ for the second one. Denote the values of the phases just before the moments of the pulses arrival as $\varphi_1^p = \varphi_1[t = (t_2^p + \tau) \mod P]$ and $\varphi_2^p = \varphi_2[t = (t_1^p + \tau) \mod P]$. Then the values of the phase shifts caused by the pulses equal $\Delta\varphi_j^p = \varepsilon\omega_j f(\varphi_j^p)$. This means that the values of the phases for $t = P$ equal

$$\varphi_1(P) = \left(P + \varepsilon\sum_{p=1}^{n} f\left(\varphi_1^p\right)\right) \mod 1 = P + \varepsilon\sum_{p=1}^{n} f\left(\varphi_1^p\right) - m,$$

$$\varphi_2(P) = \left(\eta + \omega P + \omega\varepsilon\sum_{p=1}^{m} f\left(\varphi_2^p\right)\right) \mod 1 = \eta + \omega P + \omega\varepsilon\sum_{p=1}^{m} f\left(\varphi_2^p\right) - n.$$

Provided $\varphi_1(P) = 0$, one may obtain an equation for the period P:

$$P = m - \varepsilon\sum_{p=1}^{n} f\left(\varphi_1^p\right),$$

and calculate the new phase difference $\overline{\eta} = \varphi_2(P) - \varphi_1(P)$:

$$\overline{\eta} = \eta + \omega m - n + \omega\varepsilon\left(\sum_{p=1}^{m} f\left(\varphi_2^p\right) - \sum_{p=1}^{n} f\left(\varphi_1^p\right)\right). \tag{2}$$

This equation is a Poincaré map governing dynamics of the phase difference η in the vicinity of the periodical solution. The regime of $m:n$ synchronization corresponds to a stable fixed point of the map (2). Let us study the map (2) for small $\varepsilon \to 0$. It is easy to see that for $\varepsilon = 0$,

$$t_1^p = p,$$
$$t_2^p = \frac{p-\eta}{\omega_2},$$
$$\varphi_1^p = t_2^p + \tau = \frac{p-\eta}{\omega} + \tau, \tag{3}$$
$$\varphi_2^p = \eta + \omega\left(t_1^p + \tau\right) = \eta + \omega(p+\tau). \tag{4}$$

The map (2) reduces to

$$\overline{\eta} = \eta + \omega m - n,$$

which has a (neutrally) stable fixed point for $\omega = n/m$. For $0 < \varepsilon \ll 1$ variations of φ_j^p with respect to the values (3) and (4) are of the order of ε, and the map (2) transforms into

$$\overline{\eta} = \eta + \omega m - n + \omega\varepsilon\left\{\sum_{p=1}^{m} f[\eta + \omega(p+\tau)] - \sum_{p=1}^{n} f\left(\frac{p-\eta}{\omega} + \tau\right)\right\} + O(\varepsilon^2),$$

which implies $\omega = n/m + O(\varepsilon)$ and allows further simplification:

$$\overline{\eta} = \eta + \omega m - n + \varepsilon\omega S_\tau^{mn}(\eta), \tag{5}$$

where

$$S_\tau^{mn}(\eta) = \sum_{p=1}^{m} f\left(\eta + \frac{n}{m}(p+\tau)\right) - \sum_{p=1}^{n} f\left(\frac{m}{n}(p-\eta) + \tau\right),$$

the terms $O(\varepsilon^2)$ omitted. The shape of the function $S_\tau^{mn}(\eta)$ depends on the shape of the PRC $f(\varphi)$, as well as the values of m, n, and the delay τ. In Fig. 1(b) a typical series of return functions of the map (5) is plotted for different values of ω and fixed values of the other parameters. When ω is increased the curve moves upwards and pairs of stable and unstable fixed points appear and vanish sequentially. The synchronization is possible when at least one stable fixed point exists which implies the following condition:

$$\frac{m}{n} + \frac{\varepsilon A_\tau^{mn}}{n} \leqslant \mu \leqslant \frac{m}{n} + \frac{\varepsilon B_\tau^{mn}}{n}, \tag{6}$$

where $\mu \equiv 1/\omega$ is the autonomous period of the second oscillator, $A_\tau^{mn} := \sup_{\eta\in(0,1)} S_\tau^{mn}(\eta)$ and $B_\tau^{mn} := \inf_{\eta\in(0,1)} S_\tau^{mn}(\eta)$. The double inequality (6) defines the so-called synchronization zone—the area in the parameter space inside which $m:n$ synchronization is observed.

One may notice a number of general properties of the synchronization zones. First, for all m and n the functions A_τ^{mn} and B_τ^{mn} are 1-periodical functions of τ. This implies that the zones exist for arbitrary large coupling delay and the borders of the zones are periodical with period 1. Secondly, the width of all the zones grows linearly with the coupling strength ε. The shape of the zones depends on specificity of the PRC $f(\varphi)$, but these two properties hold true for arbitrary PRC: (1) periodical dependency on the delay and (2) linear dependency on the coupling strength.

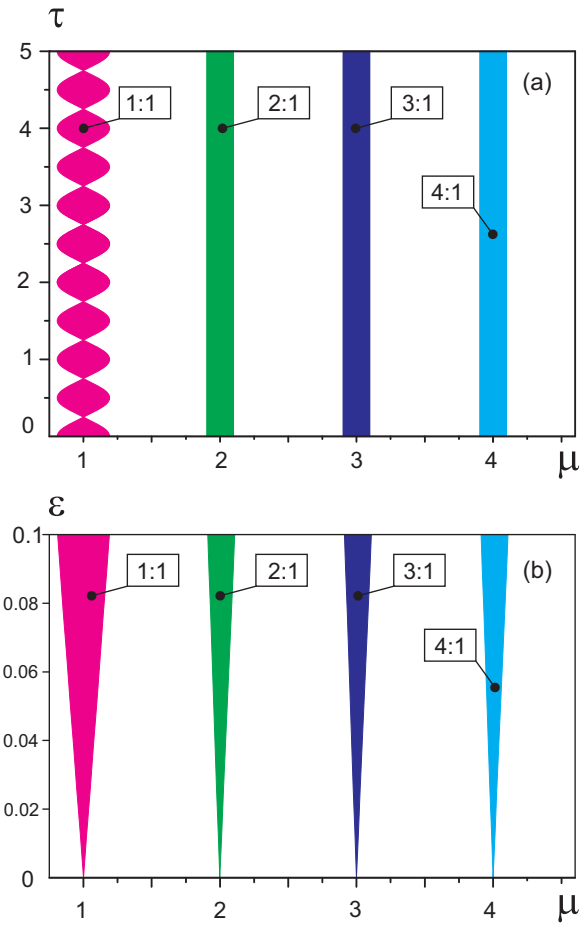

FIG. 2. (Color online) Synchronization zones for the sinusoid PRC $f(\varphi) = -\sin(2\pi\varphi)$. The rotation numbers of the zones are given in the bars. (a) The plane μ-τ for the fixed value of $\varepsilon = 0.1$. (b) The plane μ-ε for the fixed value of $\tau = 0.5$.

The exact shape of the synchronization zones depends on the particular form of the PRC. For example, suppose $f(\varphi) = -\sin(2\pi\varphi)$. This allows one to calculate $S_\tau^{mn}(\eta)$ as follows:

$$S_\tau^{mn}(\eta) = \begin{cases} -2\sin(2\pi\eta)\cos(2\pi\tau) & \text{if} \quad m = n = 1, \\ \sin[2\pi(\tau - m\eta)] & \text{if} \quad m > 1, n = 1, \\ 0 & \text{if} \quad m > n > 1, \end{cases}$$

which corresponds to the following form of synchronization zones:

$$\begin{array}{ll} |\mu - 1| \leqslant 2\varepsilon|\cos 2\pi\tau| & \text{for} \quad m = n = 1, \\ |\mu - m| \leqslant \varepsilon & \text{for} \quad m > n = 1, \\ |\mu - \frac{m}{n}| = 0 & \text{for} \quad m > n > 1. \end{array}$$

Surprisingly, the borders of all the zones except the main one do not depend on τ. The other unexpected feature is that only zones $m:1$ are observed, while the zones with $m > n > 1$ have zero width up to $O(\varepsilon^2)$. However, both these features are only due to sinusoid PRC and may be not the case for other types of PRC. The synchronization zones for the sinusoid PRC are depicted in Fig. 2.

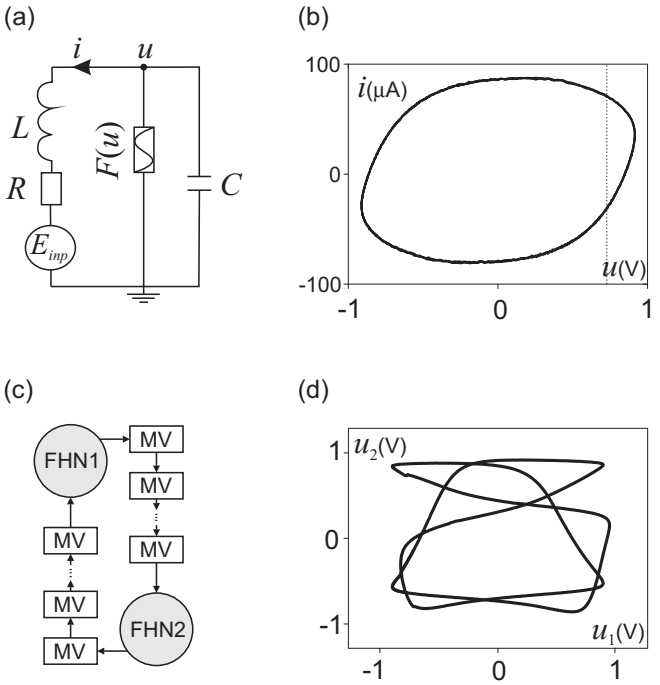

FIG. 3. Experimental setup. (a) The circuitry of the FHN oscillator. (b) The phase plane of the FHN oscillator: the current i versus the voltage u. The dashed line shows the threshold for the output pulse. (c) The circuitry of two oscillators coupled via two delay lines. (d) The Lissajous figure for 3:2 synchronization of the oscillators: the output voltages u_2 versus u_1.

III. EXPERIMENTAL STUDY OF THE SYSTEM

The next step of our study was experimental testing of the theoretical results. For this sake we designed an electronic circuit mimic. We used the FitzHugh-Nagumo (FHN) system [21] in suprathreshold regime as a base unit for the oscillatory network. This system was previously implemented as an electronic circuit [22] depicted in Fig. 3(a). Here u is the voltage on the capacitor, i is the current through the inductor, $F(u) = \alpha u(u - u_0)(u + u_0)$ is the current-voltage characteristic of the nonlinear resistor, and E_{inp} is the input signal. The parameter values were set as $R = 1\ \text{k}\Omega$, $\alpha = 2.02 \times 10^{-4}\ \Omega^{-1}\,\text{V}^{-2}$, and $u_0 = 0.82$ V. The capacitance C and the inductance L were the control parameters governing the oscillation period T. The dynamics of an isolated FHN oscillator is illustrated in Fig. 3(b). Its only attractor is the limit cycle.

The full experimental setup is depicted in Fig. 3(c) and consists of two FHN oscillators with pulse coupling via two delay lines. To perform pulse coupling we used a monostable multivibrator which fires when the output voltage of the oscillator u exceeds the threshold u_{th}. In this moment the oscillator produces a pulse which starts to travel through the delay line to the other oscillator. The circuitry of the delay lines is conditioned by their limited function, i.e., by the fact that they are designed to convey not arbitrary signals, but only series of pulses. Each delay line was realized as a chain of monostable multivibrators connected successively (compare with [23]). When an input pulse arrives to the first multivibrator it fires and produces an output pulse. Its falling edge activates the second multivibrator, which in turn activates the third one, and so on. Finally the last multivibrator fires producing the output pulse which is applied to the target oscillator. If the chain consists of N monostable multivibrators with duration d each, the total delay of the line equals $D = Nd$. The resolution of the delay line is d meaning that it is able to resolve two input pulses arriving with time lag $\Delta t > d$ one after another. The input pulse received by the target oscillator from the delay line has a square shape with amplitude E and duration $\theta \ll T$.

We studied the dynamics of the two oscillators for various frequency mismatch and coupling parameters. The internal parameters of the first oscillator were fixed to $C_1 = 47$ nF and $L_1 = 9.4$ H, which corresponds to the period $T_1 = 5$ ms. The parameters of the second oscillators were changed proportionally so that $C_2 = \mu C_1$ and $L_2 = \mu L_1$. This ensured that the shape of the limit cycle was fixed and only its period changed: $T_2 = \mu T_1$. The values of the delays were set equal for both lines. The duration of the input pulses was fixed and the same for the both oscillators: $\theta = 0.05$ ms. The coupling strength was controlled by the pulse amplitude E. Thus, the control parameters of the system were the period of the second oscillator $T_2 \equiv T$, the coupling delay D, and the coupling strength E.

To detect synchronization between the oscillators we used the technique based on Lissajous figures which we observed on an oscilloscope with u_1 on the horizontal axis and u_2 on the vertical one. For $m:n$ synchronization, the Lissajous figure has m horizontal lobes and n vertical lobes. To determine the parameter area corresponding to this regime we started from some point belonging to it and changed the parameters until the Lissajous figure collapsed. An example of the Lissajous figure for 3:2 synchronization is given in Fig. 3(d).

The main experimental results are shown in Fig. 4 where experimentally obtained bifurcation diagrams of the synchronous regimes are presented. We investigated 1:1, 2:1, 3:1, 4:1, 3:2, and 4:3 synchronization. White areas correspond to asynchronous regimes or synchronization with rotation numbers different from those listed above. The most remarkable result is that a synchronous regime with any rotation number can be observed for very large coupling delays. In Fig. 4(a) the delay D is varied from zero to 25 ms, which is only five times larger than the smaller period, but we also obtained synchronization for the delay values up to ~500 ms, i.e., $D \sim 100T$. The width of the zones depends on E linearly and depends on D periodically, in agreement with the theory. However, the zone borders are not strictly periodical, which is most clearly seen for the 1:1 zone which gets skewed as D grows.

In order to compare the experimental results and the theoretical predictions we determined the phase resetting curve of the FHN oscillator. To obtain the PRC we first need to define the phase φ of the unperturbed oscillator. The easiest way to define it is through the moments when the oscillator reaches the threshold and emits pulses. Denote these moments as $\{t_n\}$, $n \in \mathbf{Z}$, then for $t \in [t_n; t_{n+1}]$ the phase φ is defined as

$$\varphi = \frac{t_{n+1} - t}{t_{n+1} - t_n} = \frac{t_{n+1} - t}{T},$$

where $T = t_{n+1} - t$ is the unperturbed length of the cycle. The phase value defines the position of the oscillator on the limit

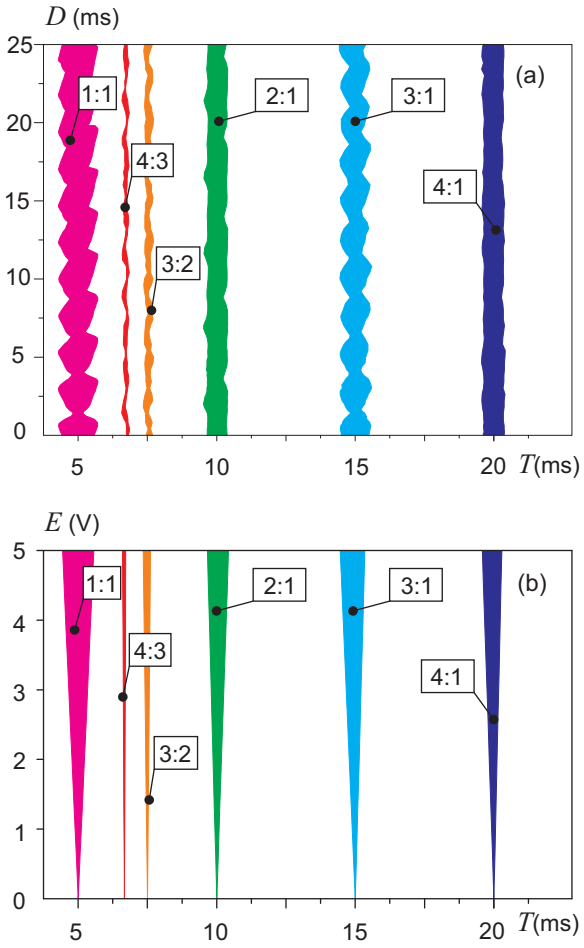

FIG. 4. (Color online) The experimentally obtained synchronization zones for two FHN oscillators. The rotation numbers of the zones are given in the bars. (a) The plane T-D for the fixed value of $E = 5$ V. (b) The plane T-E for the fixed value of $D = 2.5$ ms.

cycle and changes from 0 to 1. When the phase reaches unity it resets to zero and the oscillator produces a pulse.

The PRC of the oscillator $F(\varphi)$ is defined as the phase shift caused by the input pulse applied to the oscillator when its phase equals φ:

$$F(\varphi) = \Delta\varphi = \frac{T - T_1}{T}, \tag{7}$$

where T_1 is the length of the cycle in which the perturbing pulse is applied. The definition of the phase resetting curve is illustrated in Fig. 5(a).

Figure 5(b) presents the PRC obtained experimentally for the FHN oscillator. This PRC is of the second type [24] and resembles a distorted sinusoid. To test different strengths of the pulse coupling we fixed the input pulse length $\theta = 0.05$ ms and varied the amplitude E. It was shown that the shape of the PRC does not change much for $E \leqslant 5$ V, and its magnitude scales linearly [Fig. 5(c)]. The other important observation is that the PRC magnitude scales inversely linearly with the period T of the oscillations [Fig. 5(d)]. These observations allow us to use the following expression for the PRC:

$$F(\varphi) = \varepsilon\omega f(\varphi),$$

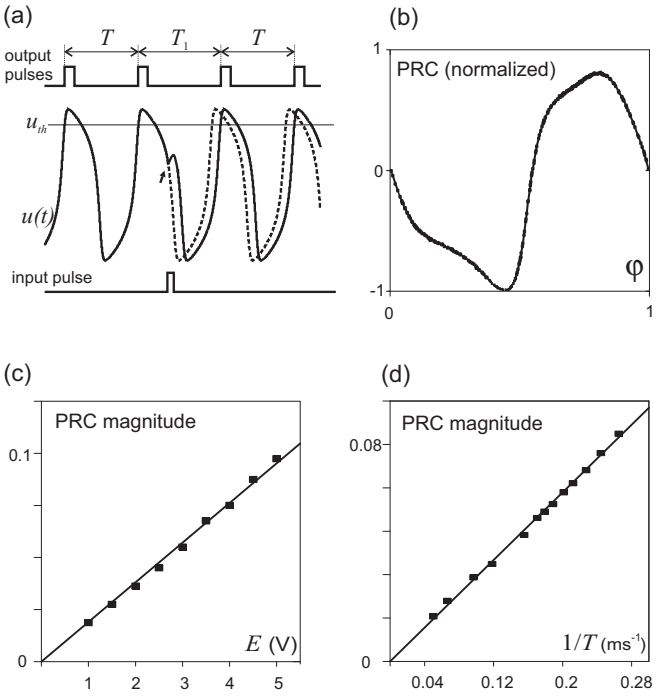

FIG. 5. (a) Definition of the PRC: An external pulse is applied to the oscillator and the perturbed period is measured. (b) The normalized PRC of the FHN oscillator. (c) Linear dependency between the magnitude of the PRC and the pulse amplitude E (for $T = 5$ ms). (d) Inversely linear dependency between the magnitude of the PRC and the period of the oscillator (for $E = 5$ V).

where $\varepsilon = E/E_0$, $\omega = T_0/T$, $f(\varphi)$ is the normalized PRC, and the constants $E_0 = 64$ V and $T_0 = 5$ ms.

Using the obtained PRC for the FHN oscillator we calculated the borders of the synchronization zones according to (6). These borders are plotted in Fig. 6 by solid lines together with the experimental borders depicted by squares. Different colors of lines and squares correspond to different rotation numbers (see the legend). One can see that the experimental results match the theoretical predictions quite well which indicates the reliability of the developed theory.

In order to carry out a control experiment to challenge the developed theory we decided to study more subtle dynamical effects, namely, bifurcations inside the synchronization zones. We noticed that smooth change of the parameters, for example the coupling delay, *inside* the synchronization zone, sometimes leads to fast switch between different regimes of synchronization of the same order. An example of this effect is given in Fig. 7(a) in which the periods of the oscillators are tuned as 2:1. For the delay range 3.06 ms $\leqslant D \leqslant$ 3.4 ms two different Lissajous figures are observed. Both of these figures correspond to synchronization 2:1, with different phase relationships between the oscillators. Thus, the system demonstrates bistability in a certain parameter interval. The switching between the regimes occurs on the borders of the bistability interval and has hysteresis nature.

After experimental observation of the system bistability we checked if the developed theory can predict this effect. For this sake we constructed the map (5) for the parameters inside the bistability interval. This map is plotted in Fig. 7(b). One can

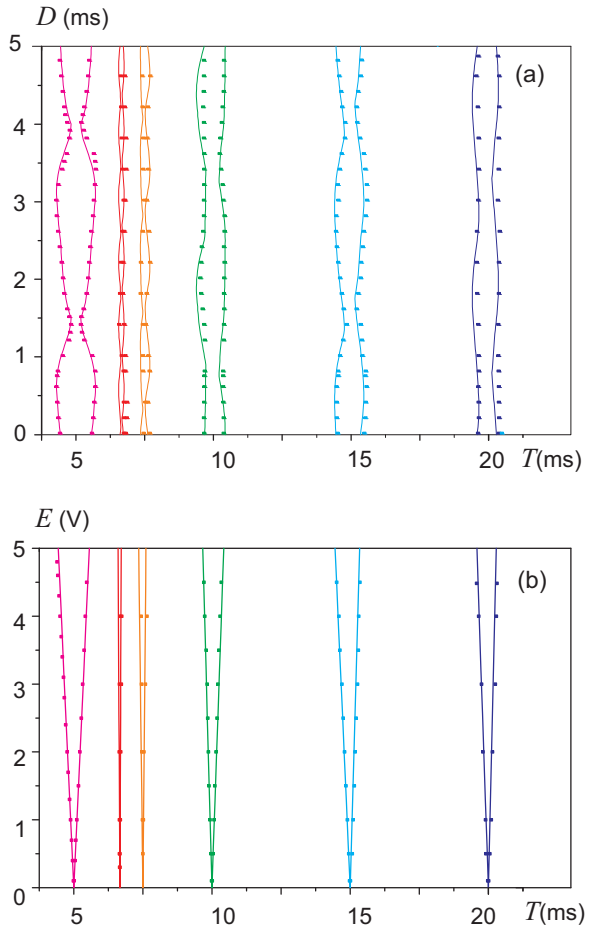

FIG. 6. (Color online) The borders of the synchronization zones: theoretical predictions (solid lines) and experimental results (dots). (a) The plane T-D for the fixed value of $E = 5$ V. (b) The plane T-E for the fixed value of $D = 2.5$ ms.

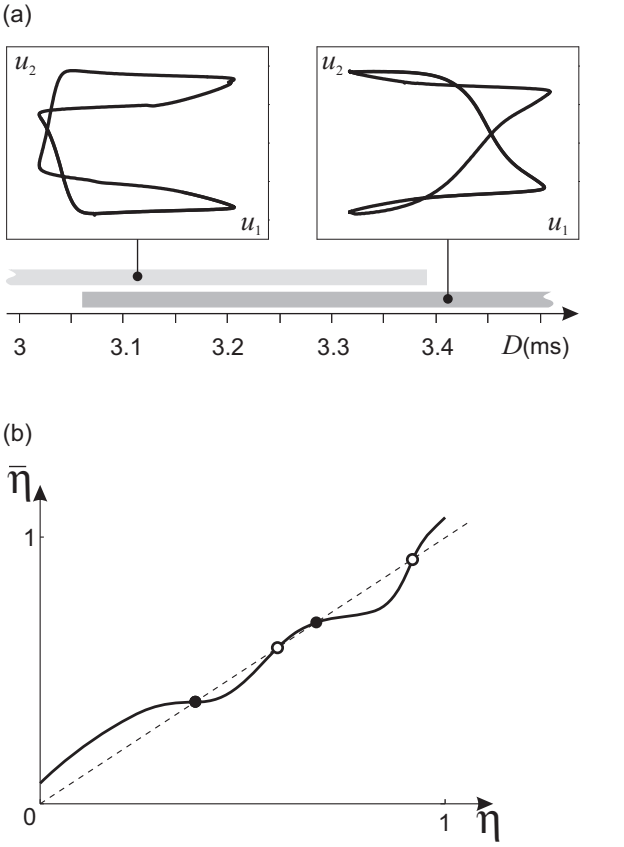

FIG. 7. (a) Bistability of the system: the Lissajous figures for two different regimes of 2:1 synchronization (top) and the delay intervals in which they exist (bottom). (b) The map (5) in the interval of bistability has two stable (solid circles) and two unstable (empty circles) fixed points.

see that it has exactly two stable fixed points corresponding to different regimes of synchronization. On the borders of the bistability interval one of the stable fixed points vanishes through a saddle-node bifurcation, and the system switches to another one.

IV. DISCUSSION

We have considered cross-frequency synchronization of two oscillators with time-delayed pulsatile coupling. We studied the case of symmetric delays, which, however, can be easily generalized for the asymmetric case [25]. Both theoretical and experimental study have been carried out. Our theoretical study is based on the concept of PRCs. In the framework of this concept we constructed a Poincaré map describing the dynamics of the investigated system. Synchronous regimes of the system correspond to stable fixed points of the map. In the limit of weak coupling we derived the explicit form of the Poincaré map and obtained the synchronization zones, i.e., the areas in the parameter space inside which the synchronization takes place.

The most interesting fact about the synchronization zones is that they last to infinity along the τ axis. This means that synchronization with arbitrary rotation number is possible for arbitrary large coupling delays. Moreover, the width of the synchronization zone is a periodical function of the delay. For a special case of the sinusoid PRC this width is constant for $m > n = 1$ and very small $[O(\varepsilon^2)]$ for $m > n > 1$. For nonsinusoid PRCs all the zones have a width of the order of ε, and the borders of all the zones are periodical with respect to τ. However, the zones with $m > n = 1$ typically remain wider than the zones with $m > n > 1$. For example, for the PRC from Fig. 5(b) the widths of the zones along the μ axis are given by Table I. One can see that the zones with $\rho = 3:2$ and $\rho = 4:3$ are much narrower than the other ones.

TABLE I. Theoretical and experimental widths of the synchronization zones for $\tau = 1$, $\varepsilon = 0.078$ ($D = 5$ ms, $E = 5$ V).

Rotation number	Theoretical width	Experimental width	Mismatch
1:1	0.232	0.232	0.2%
4:3	0.024	0.014	41%
3:2	0.054	0.062	15%
2:1	0.156	0.141	11%
3:1	0.183	0.185	1%
4:1	0.144	0.161	11%

Another noteworthy feature of the synchronization zones is the linear dependency of their width on the coupling strength ε for all rotation numbers ρ. This feature is probably due to the pulsatile nature of coupling in the system, because typically cross-frequency synchronization with $\rho \neq 1$ is observed only in narrow parameter areas. For example, in the classical sinusoid circle map the zone with rotation number $m:1$ has a width of the order of ε^m [26,27]. In our system in the case of the sinusoid coupling function the width of the synchronization zones is of the order of ε for all rotation numbers.

To challenge the developed theory for cross-frequency synchronization we developed an electronic circuit implementing two FHN oscillators coupled via delay lines. We note that the circuitry of the delay lines was determined by their limited function, i.e., conveying only pulsatile signals. However, this allowed one to use a quite simple schematic instead of expensive digital delay lines. In our circuit we obtained cross-frequency synchronization with various rotation numbers and confirmed that it is observed for quite large coupling delays (100 times larger than the period of the faster oscillator). We also confirmed linear dependency of the synchronization zones on the coupling strength and their periodical dependency on the coupling delay. However, the latter dependency is not strictly periodical: The borders of the zones get skewed when the coupling delay grows.

Thus, the developed theory is qualitatively confirmed by the experiment. To make a quantitative comparison of the theoretical predictions and the experimental results we determined the PRC for a FHN oscillator and constructed the synchronization zones for this PRC. The results of the comparison are depicted in Fig. 6 from which one can see that the theoretical and experimental borders of the synchronization zones agree quite well. To assess the agreement numerically the values of the theoretical and experimental widths of the zones are given in Table I. From this table one can see that the widths of the $m:1$ zones are predicted by the theory with satisfactory accuracy ($\lesssim$10% for $\varepsilon = 0.08$). However, the widths of the zones with $m > n > 1$ are predicted with much worse accuracy ($>40\%$ for the zone $4:3$), so one may speak only of a qualitative description of these zones.

A number of reasons may lead to the observed discrepancy between the theory and the experiment. First, the PRC formalism does not describe the dynamics of the circuit precisely. When an external pulse acts on the oscillator the perturbations may not completely vanish during the first period as is supposed in the PRC-based approach but may influence the next period as well. This influence is described by the so-called second order phase resetting curve (PRC2). For the FHN oscillator the PRC2 may reach the level of about 5% of the PRC magnitude. Secondly, the developed theory is valid in the limit of weak coupling since the terms $O(\varepsilon^2)$ are omitted in (5). In the experiments we used coupling strengths of the order $\varepsilon \sim 0.1$. Thus, relative accuracy of the order of 10% is satisfactory. The accuracy should decay for zones with larger values of m and n because for such zones the actual values of φ_j^p in (2) deviate significantly from the values given by (3) and (4). For a similar reason the accuracy of the theoretical predictions should decay with the growth of the delay: The error is accumulated through a number of periods while pulses travel from one oscillator to another. And the most dramatic fall of the accuracy is observed for the zones with $m > n > 1$: These zones are relatively narrow and probably the higher-order terms make a significant contribution to their width.

Note added. Recently we learned about the novel results from the group of Vanag who studied the dynamics of coupled chemical oscillators. Their previous results mostly rely on numerical simulations [15], and recently they were confirmed and refined by the experiment [28]. The observed phenomena include cross-frequency synchronization of two chemical oscillators in the presence of significant coupling delays. Unfortunately, the accuracy of the experiments did not allow the authors to study the detailed structure of the borders of the synchronization zones. The authors also found a more subtle effect which we observed as well, namely, the coexistence of multiple synchronous regimes with the same rotation number. These regimes are characterized by different phase relations between the oscillators, similarly to the case depicted in Fig. 7. When the delay slowly changes the system can switch from one regime to another, so that the phase shift between the oscillators undergoes an abrupt jump. Such type of behavior observed for both electronic and chemical oscillators seems to be typical for oscillators with time-delayed coupling. The described effect may be considered as a generalization of what is known as the phase-flip bifurcation observed earlier for $1:1$ synchronization [29].

In conclusion, we studied cross-frequency synchronization of oscillators with time-delayed pulsatile coupling. In the theoretical part of the paper we constructed a Poincaré map describing the synchronization properties including location of the synchronization zones in the parameter space and bifurcations of the synchronous regimes inside the zones. In the experimental part we designed an electronic circuit demonstrating the investigated phenomenon. The obtained experimental and theoretical results are in good agreement and confirm each other.

ACKNOWLEDGMENTS

The theoretical study was carried out with financial support from the Russian Science Foundation (Project No. 14-12-01358). The experimental study was carried out with financial support from the Russian Foundation for Basic Research (Grants No. 13-02-97050, No. 14-02-00042, and No. 14-02-31873).

[1] I. I. Blekhman, *Synchronization in Science and Technology* (ASME Press, New York, 1988); S. H. Strogatz, D. M. Abrams, A. McRobie, B. Eckhardt, and E. Ott, Nature (London) **438**, 43 (2005).

[2] A. E. Siegman, *Lasers* (University Science Books, Mill Valley, CA, 1986); R. Roy and K. S. Thornburg, Phys. Rev. Lett. **72**, 2009 (1994).

[3] W. C. Lindsey, *Synchronization Systems in Communication and Control* (Prentice-Hall, Englewood Cliffs, NJ, 1972); L. Kocarev, K. S. Halle, K. Eckert, L. O. Chua, and U. Parlitz, Int. J. Bifurcation Chaos Appl. Sci. Eng. **02**, 709 (1992); A. S. Dmitriev, G. A. Kassian, and A. D. Khilinsky, *ibid.* **10**, 749 (2000).

[4] Y. Kuramoto, *Chemical Oscillations, Waves, and Turbulence* (Springer-Verlag, Berlin/New York, 1984).

[5] A. T. Winfree, *The Geometry of Biological Time* (Springer-Verlag, New York, 2001); L. Glass, Nature (London) **410**, 277 (2001).

[6] W. Singer, Annu. Rev. Phys. **55**, 349 (1993); Neuron **69**, 191 (2011).

[7] C. M. Gray, P. König, A. K. Engel, and W. Singer, Nature (London) **338**, 334 (1989).

[8] J. Sarnthein, H. Petsche, P. Rappelsberger, G. L. Shaw, and A. Von Stein, Proc. Natl. Acad. Sci. USA **95**, 7092 (1998); W. Klimesch, Int. J. Psychophysiol. **24**, 61 (1996).

[9] V. B. Kazantsev, V. I. Nekorkin, V. I. Makarenko, and R. Llinas, Proc. Natl. Acad. Sci. USA **101**, 18183 (2004); A. J. Ijspeert, Neural Networks **21**, 642 (2008).

[10] C. Hammond, H. Bergman, and P. Brown, Trends Neurosci. **30**, 357 (2007); P. J. Uhlhaas and W. Singer, Nat. Rev. Neurosci. **11**, 100 (2010).

[11] J. R. Isler, P. G. Grieve, D. Czernochowski, R. I. Stark, and D. Friedman, Brain Res. **1232**, 163 (2008); P. Sauseng, W. Klimesch, W. Gruber, M. Doppelmayr, W. Stadler, and M. Schabus, Neurosci. Lett. **324**, 121 (2002); P. Sauseng, W. Klimesch, W. R. Gruber, and N. Birbaumerb, Neuroimage **40**, 308 (2008).

[12] V. V. Klinshov and V. I. Nekorkin, Phys. Usp. **56**, 1217 (2013); E. Schöll, *Advances in Analysis and Control of Time-Delayed Dynamical Systems*, edited by J.-Q. Sun and Q. Ding (World Scientific, Singapore, 2013), p. 57.

[13] T. Heil, I. Fischer, W. Elsasser, J. Mulet, and C. R. Mirasso, Phys. Rev. Lett. **86**, 795 (2001); H.-J. Wünsche, S. Bauer, J. Kreissl, O. Ushakov, N. Korneyev, F. Henneberger, E. Wille, H. Erzgräber, M. Peil, W. Elsasser, and I. Fischer, *ibid.* **94**, 163901 (2005); R. Vicente, S. Tang, J. Mulet, C. R. Mirasso, and J.-M. Liu, Phys. Rev. E **73**, 047201 (2006); I. Fischer, R. Vicente, J. M. Buldú, M. Peil, C. R. Mirasso, M. C. Torrent, and J. Garcıá-Ojalvo, Phys. Rev. Lett. **97**, 123902 (2006).

[14] S. Heiligenthal, T. Dahms, S. Yanchuk, T. Jüngling, V. Flunkert, I. Kanter, E. Schöll, and W. Kinzel, Phys. Rev. Lett. **107**, 234102 (2011); T. Jüngling, H. Benner, H. Shirahama, and K. Fukushima, Phys. Rev. E **84**, 056208 (2011); L. Weicker, T. Erneux, L. Keuninckx, and J. Danckaert, *ibid.* **89**, 012908 (2014).

[15] V. Horvath, P. L. Gentili, V. K. Vanag, and I. R. Epstein, Angew. Chem. Int. Ed. **51**, 6878 (2012); A. I. Lavrova and V. K. Vanag, Phys. Chem. Chem. Phys. **16**, 6764 (2014).

[16] L. Glass and J. Sun, Phys. Rev. E **50**, 5077 (1994); S. Coombes and P. C. Bressloff, *ibid.* **60**, 2086 (1999); A. P. Kuznetsov, N. V. Stankevich, and L. V. Tyuryukina, Tech. Phys. Lett. **32**, 343 (2006); Physica D Nonlinear Phenom. **238**, 1203 (2009); C. C. Canavier, F. G. Kazanci, and A. Prinz, Biophys. J. **97**, 59 (2009).

[17] C. Canavier and S. Achuthan, Math. Biosci. **226**, 77 (2010).

[18] W. Gerstner, Phys. Rev. Lett. **76**, 1755 (1996); U. Ernst, K. Pawelzik, and T. Geisel, *ibid.* **74**, 1570 (1995); Phys. Rev. E **57**, 2150 (1998); S. Coombes and G. J. Lord, *ibid.* **56**, 5809 (1997); **55**, R2104 (1997); G. B. Ermentrout and N. Kopell, Proc. Natl. Acad. Sci. USA **95**, 1259 (1998); M. Zeitler, A. Daffertshofer, and C. C. A. M. Gielen, Phys. Rev. E **79**, 065203 (2009); M. Woodman and C. Canavier, J. Comput. Neurosci. **31**, 401 (2011); V. V. Klinshov and V. I. Nekorkin, Chaos, Solitons Fractals **44**, 98 (2011); Cybern. Phys. **1**, 106 (2012); J. Discont., Nonlinearity Complexity **1**, 253 (2012).

[19] V. V. Klinshov and V. I. Nekorkin, Commun. Nonlinear Sci. Numer. Simulat. **18**, 973 (2013).

[20] Consider a system $\gamma\dot{x} = f(x) + \varepsilon\delta(t)$, where x is a vector and $\varepsilon\delta(t)$ is the input pulse signal. Suggest that in the autonomous case ($\varepsilon = 0$) the system has a limit cycle, then its period is proportional to γ. The input pulse causes an instant state shift whose size equals ε/γ. Thus, if the system remains in the vicinity of the limit cycle, the phase shift is proportional to the pulse magnitude and to the natural frequency of the oscillations.

[21] R. Fitzhugh, Biophys. J. **1**, 445 (1961); J. Nagumo, S. Arimoto, and S. Yoshizawa, Proc. IRE **50**, 2061 (1962).

[22] D. S. Shchapin, J. Commun. Technol. Electron. **54**, 175 (2009).

[23] D. P. Rosin, D. Rontani, D. J. Gauthier, and E. Schöll, Europhys. Lett. **100**, 30003 (2012); Phys. Rev. Lett. **110**, 104102 (2013).

[24] D. Hansel, G. Mato, and C. Meunier, Neural Comput. **7**, 307 (1995).

[25] L. Lücken, J. P. Pade, K. Knauer, and S. Yanchuk, Europhys. Lett. **103**, 10006 (2013).

[26] V. I. Arnold, Russ. Math. Surv. **38**, 215 (1983).

[27] A. Pikovsky, M. Rosenblum, and J. Kurths, *Synchronization: A universal Concept in Nonlinear Sciences* (Cambridge University Press, Cambridge, 2001).

[28] I. S. Proskurkin and V. K. Vanag, Russian J. Phys. Chem. A (Zh. Fi. Khim.) **89** (2015), doi:10.1134/S0036024415020223.

[29] A. Prasad, S. K. Dana, R. Karnatak, J. Kurths, B. Blasius, and R. Ramaswamy, Chaos **18**, 023111 (2008).